New beam-to-beam joint with concrete embedding for composite bridges Experimental study and finite element modelling

Hugues Somja, Kaing Sao Serey, Alain Lachal

NEW BEAM-TO-BEAM JOINT WITH CONCRETE EMBEDDING FOR COMPOSITE BRIDGES

Experimental Study and Finite Element Modelling

Hugues Somja[1], SaoSerey Kaing[1] and Alain Lachal[1]

[1] National Institute of Applied Sciences, Rennes, France

ABSTRACT

This paper deals with a new type of beam-to-beam joint used to connect continuously composite beams in small and medium span bridges. This new joint is realized by encasing totally the two composite beam ends into a massive composite reinforced concrete block. A direct contact between the ends of the bottom flanges of the steel girders over the support ensures the transfer of the compression forces. A half-scale joint specimen has been designed and fabricated. The specimen was first tested at the Structural Laboratory of INSA-Rennes under fatigue loading. Next, the load was monotonically increased up to the specimen failure. The main results of this experimental study are firstly presented. To allow an accurate interpretation of the test results and get a better insight into the joint behaviour, a numerical F.E. model has been developed. The numerical results are presented and compared against experimental ones. Besides, a parametric study has been carried out in order to investigate the influence of key parameters governing the joint behaviour. The influence of the behaviour of this type of joint on the global analysis of a continuous composite beam has then been studied. Finally, a worked exemple of a two-span continuous railwayl bridge is presented and effects of intermediate beam-to-beam joint characteristics on the bridge behaviour are discussed.

KEYWORDS

Composite bridge, beam-to-beam connection, embedded joint, shear connection, direct contact, F.E. model

1 INTRODUCTION

Bridges with span lengths of 15 m to 30 m are common in practice and they have been mostly built in the past adopting concrete or prestressed concrete solutions. In order to promote composite solutions, research programs have been developed, with the main objective to find innovative solutions to make composite bridge superstructures cost competitive, as much as possible, with ordinary prefabricated elements easily assembled on site by the same builder with a minimum of construction operations and without any sophisticated technology (such as outdoor welding for example).

The first researches on this topic were developed in Australia between 1974 and 1991 (see [1] to [6]) upon request of the Department of Main Roads of Western Australia. In the same period several composite bridges were also built in the United States. More recently, in Europe, researches were carried out by J. Wang, R. Baus and A. Bruls (1997) [7], J. Haensel (2001) [8] in East Germany and through a research project, RWTH-CTICM-PROFILARBED (2000-2003) [9] where new joint solutions were proposed considering aspects such as strength and fatigue of hybrid girders, use of dismountable shear anchors, use of prefabricated elements…

Within this context, under the impulse of the French Research Project MIKTI [10], several research actions have been undertaken. The Structure Laboratory of INSA Rennes was involved in this research project to investigate innovative solutions for the design and the fabrication of beam-to-beam joints ensuring the continuity of bridge composite beams [11]. Three continuous joint solutions have been selected and then studied. The aim of this paper deals with the third selected

solution. It consists in embedding the steel span girder ends of the composite slab in a massive reinforced concrete transverse beam resting on the top of the pile heads.

The steelwork parts of the composite beams are prepared in factory and equipped with steel elements for connections (plates, holes, welded studs…). Then, the steel girders are transported on the construction site to be placed on their supports. Without any proping, the steel span girders, simply supported at their ends on the head of the piles, operate like isostatic beams. The joint components (contact, studs…) and the reinforcement are installed. The slab is concreted and the continuity of the composite beam is completed by concreting the beam joints and the transverse beams over the pile. Possibly, separate supports can be considered between the transversal beam and the pile to limit the shear transfer through the joint. This novel joint appears comparable to some hybrid joints used in USA and in Japan to connect composite beam to concrete column [12].

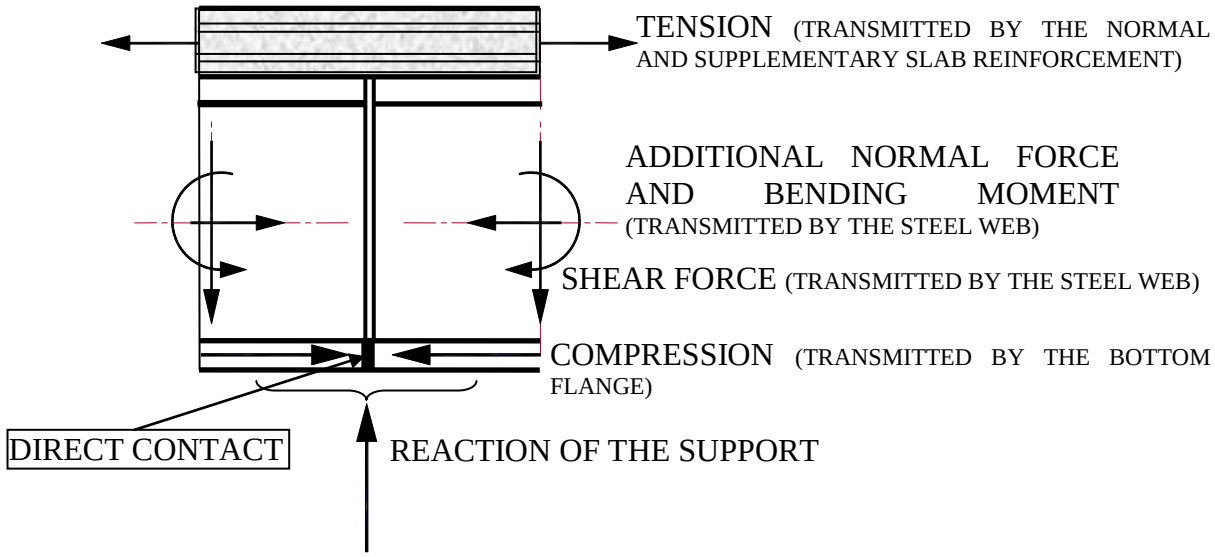

Figure 1: Internal forces transmitted by the joint

Regarding the transmission of internal forces, different parts of the joint contribute to the transfer of the bending moment, normal forces and shear forces (Fig. 1). The direct contact placed between the ends of the bottom flanges of the girders over the support ensures the transfer of the compressive forces. The transfer of the tensile forces in the upper part of the joint is ensured by a supplementary reinforcement in the slab and a supplementary shear connection between the top girder flanges and the slab. Inside the concrete embedding, reinforcement, transversal shear studs welded on the webs and/or rebars passing through the girder webs allow to transfer the shear forces as well as additional normal force and bending moment (see Fig. 2c).

Due to the three dimensional arrangement of the joint, a complex mechanical behavior could be expected. This paper shows that the force transfer through the joint remains simple and consequently provides data for the development of a simple analytical mechanical model for the design of such a beam-to-beam joint in continuous composite bridges.

For that purpose, we start with the presentation of an experimental study. After a description of the test specimen, the experimental test setup and loading procedure, the main experimental results are presented.

For an accurate interpretation of test results and a better understanding of some specific mechanical behaviours, a two-dimensional finite element model based on Finelg software [13] is created. Separated specific beam finite elements with 3 nodes are used for concrete and steel parts of the joint. It is shown that developped 2D model is able to reproduce accurately the flexural behaviour of the joint. Further, useful local informations at component level are also obtained. The relative

influence of the different components of the joint are also analysed by varying some of the governing parameters.

The paper ends by setting in prospect the behavior observed for the joint. A small span railway bridge is predesigned [14] and the effect of the joint stiffness on the global behavior of the bridge is discussed, at service and ultimate limit states.

2 EXPERIMENTAL STUDY

2.1 Joint specimen presentation

The specimen fabricated and tested at the Laboratory of Structural Mechanics (INSA of Rennes) is presented in figure 2a. It has been designed considering approximately half-scale of typical medium-span bridge. The span length has been chosen in order to obtain a realistic ratio between the shear force and the hogging bending moment transmitted over the intermediate support. The two end span steel girders are embedded in a massive reinforced concrete block located at mid-length of the specimen. This latter one represents a part of the reinforced concrete transverse beam resting on the pier head over its entire length through neoprene supports.

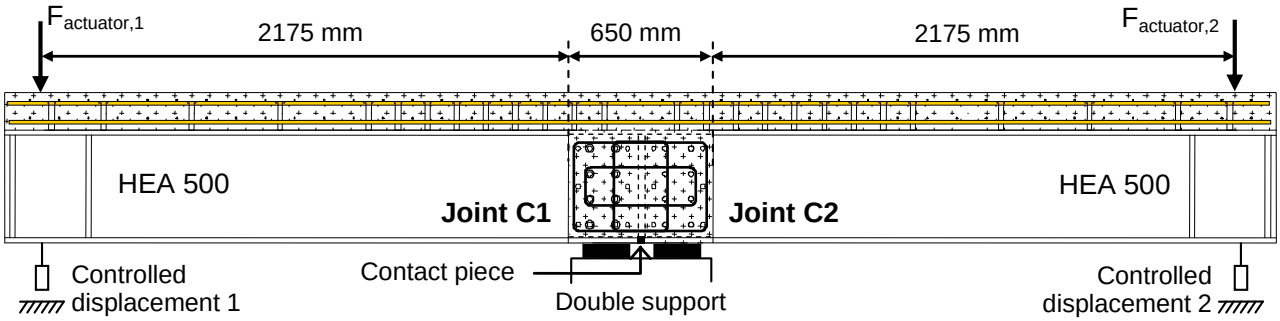

Figure 2a: Beam-to-beam joint specimen with concrete embedding

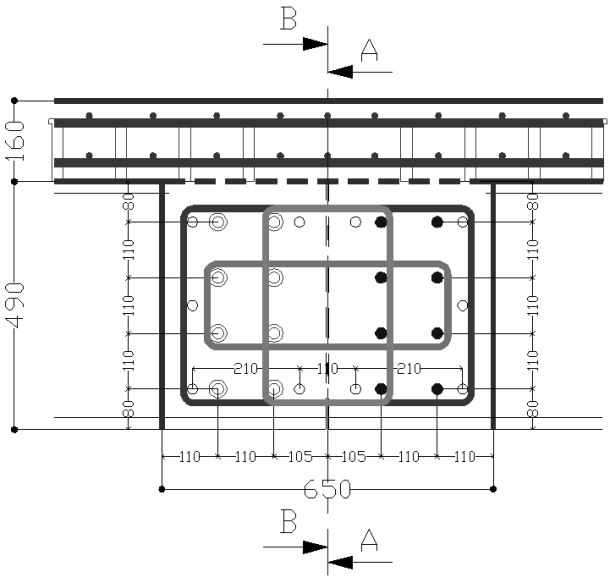

Figure 2b: Detailed view of the joint (unit: mm)

Figure 2b gives a detailed view of the joint: longitudinal and transverse reinforcement of the slab, reinforcing bars, headed studs, transverse bars and stirrups of the reinforced block. This later one can be lying either on simple or double support. In theory, the use of a double support avoids shear force transfer through the continuous joint. Actually, reaction forces are never uniformly distributed

on their support and the unsymmetrical loading action of the two spans connected on each side of the support lead to a certain shear force transfer through the concrete cross section located at mid-support. A double support was used in the case of the tested specimen shown in figures 2a.

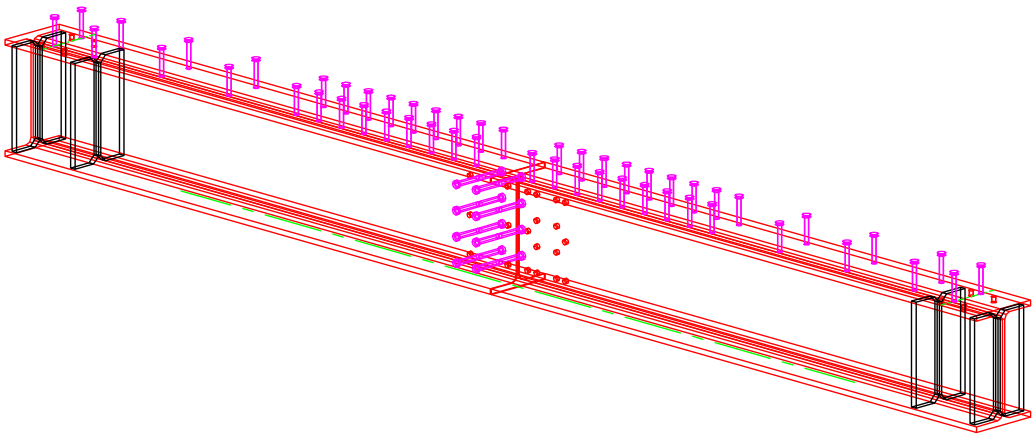

Figure 2c: 3D view of the steel part of the specimen. Web shear connection (joint C1) and predrilled holes for transverse bars (joint C2)

In fact, in a continuous joint, we have to distinguish two joints on each side of the mid-axis of the support. In figure 2a, these joints have been labeled: joint C1 on the left side (actuator 1) and joint C2 on the right side (actuator 2). The two steel span girders are HEA 500 rolled sections in steel grade S355 (E_a = 200 000 MPa, $f_{y,a}$ (web) = 450 MPa, $f_{y,a}$ (flange) = 420 MPa). They are interrupted at the mid-axis of the pile and embedded in a massive reinforced concrete block. Each end girder is set on a separate support. The contact between the ends of the bottom flanges is made by a piece of aluminum alloy (AG5) in the space left empty between the flanges of the two profile sections placed end-to-end, by means of a process similar to welding (Filcord 303C SAF welder). This product, in wire form, can be supplied quite easily (ref. Nertalic AG5; d = 1mm; batch: C21768G3 5) to satisfy standards AFNOR 81331 Al Mg5 and DIN 1732-SG Al Mg5. Experimental tests have shown that aluminum and steel in contact with each other only undergo very slight surface corrosion. Effectively, the formation of a film of corrosive products on the faces in contact, i.e. containing rust on the steel and alumina on the aluminum, obstructs the occurrence of electrochemical reaction [39].

To connect the steel girder ends inside the concrete embedding, two different arrangements have been considered (Fig. 2a, 2b and 2c). On the left side (joint C1), the web of the end steel girder is connected to the concrete block by means of 8 headed studs (d= 22 mm and h = 125 mm) welded in pairs, on each face of the steel girder web (Fig. 2c). On the right side (joint C2), shear studs welded on the web are replaced by 8 transverse bars (d=22mm) passing through predrilled holes in the web of the steel girder end (Fig. 2c). It has to be pointed out that the longitudinal reinforcement of the concrete transverse beam passing through the steel girder webs provides an additional shear resistance to that of the shear studs (joint C1) and that of the transverse bars (joint C2).

In the upper part of the joint, the transfer of the tensile forces is allowed by the shear connection and the reinforcement in the slab. The width of the slab is b^{-}_{eff} = 1600 mm and the thickness h_a = 160 mm. The strength class C45/55 is used for the concrete. The percentage of longitudinal reinforcement is 1.26 %. The reinforcement is composed of 2 layers of 8 ribbed bars of 16mm diameter with high bond action and with steel grade S500 – Category 3, ensuring high ductility. The slab is connected to the steel flange with 12 welded headed studs per span (2 lines of 6 welded headed studs; d = 22 mm, h = 125 mm, E_a = 200 000 MPa, f_y = 450 MPa). In the connected zone, the percentage of longitudinal reinforcement is increased to 2.67 % (9 additional rebars of 16mm diameter - S500 of length b_{eff} + ℓ_{bd} = 2050mm) and the number of connectors is doubled (24 studs per span).

Steel girders were prepared in factory (ArcelorMittal - Wallerich - Differdange) and equipped with holes and welded studs. They were transported to INSA in RENNES and placed on their double support. Next, the reinforcement and the contact were installed and the continuity of the composite beam was completed by concreting the slab and the joint in a single shot.

2.2 Experimental setup and loading procedure

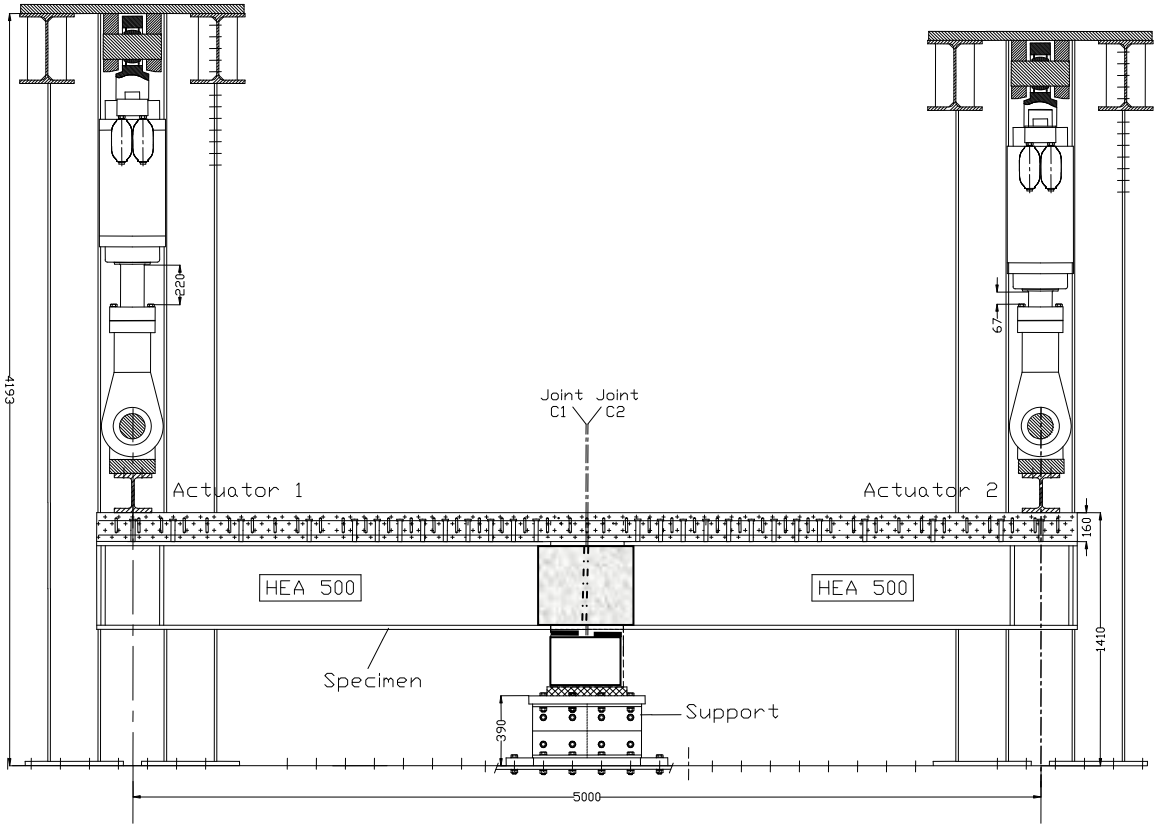

Figure 3: Test setup

The experimental setup is shown in figure 3. Two hydraulic servo controlled actuators apply two vertical loads at the beam end cross-sections of the specimen. The specimen is simply supported at mid-span resting on neoprene plates.
Two types of servo-controlled loading displacement procedure are exerted. Firstly a fatigue loading (Fig. 4) under a high range of bending moment and secondly a monotonically increase of actuator loads towards the specimen collapse.

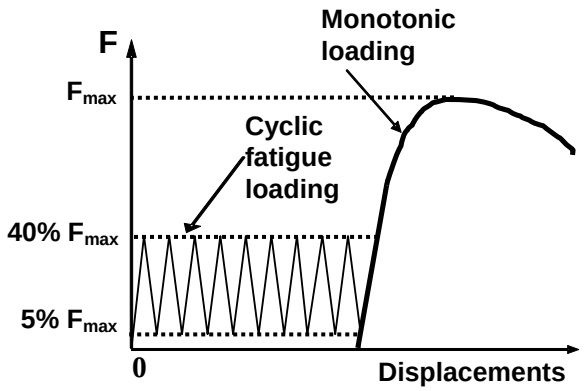

Figure 4: Loading procedure

2.3 Measure arrangement

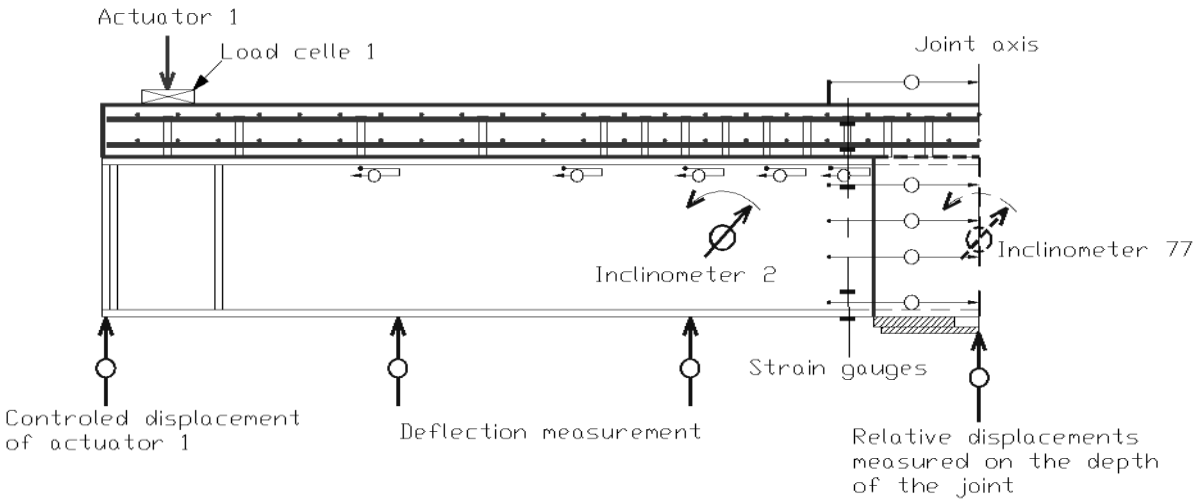

Figure 5: Measure arrangement

Figure 6: View of the specimen and the test setup

The specimens are equipped with inclinometers to measure the joint rotation. In fact, for each span, two inclinimeters are used to evaluate the relative rotation between the middle of the specimen (situated at mid-support) and a span cross-section located at 600 mm from the middle of the specimen. Linear potentiometric transducers measure deflections in several points along the beam and relative displacements at joints C1 and C2. Furthermore, one-dimensional strain gauges are used to measure strains in several parts of the specimen: steel beam, reinforcing bars, embedding reinforcement and shear connectors. Crack widths are measured on the top surface of the concrete slab. Figure 5 shows the arrangement of the main instrumentation and figure 6 gives a general view of the specimen and test setup.

2.4 Preliminary tests

Preliminary tests were carried out at INSA Rennes to make sure of the good implementation of the AG5 material between the two ends of the girder flanges (Fig. 7). Studies of the mechanical characteristics of AG5 material were also carried out. The first preliminary studies were realized on

cubic samples extracted from the material put between the flange ends. Others studies of the AG5 material were made during the test of the beam-to-beam joint specimen (Fig. 8).

Figure 7: AG5 implementation

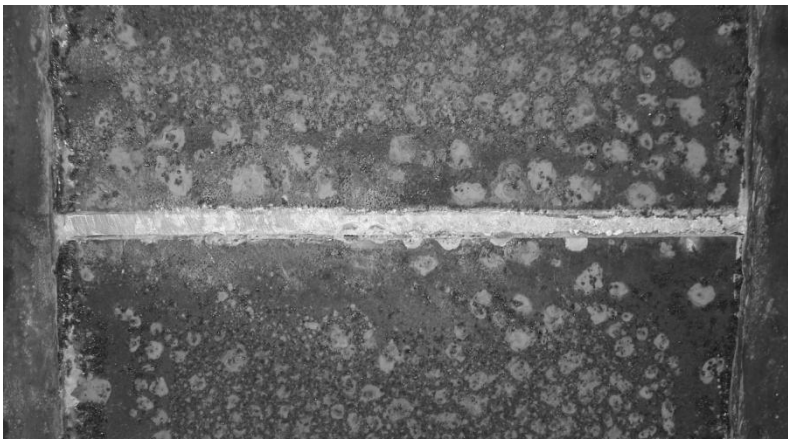

Figure 8: View of the contact piece

Figure 9 gives the skeleton curve of the force-displacement cycles recorded during the test. The force is the measured force transmitted by the girder flanges. The displacement is the relative displacement between the two ends of the girder flanges on a length equal to the thickness of the contact i.e. 10 mm.

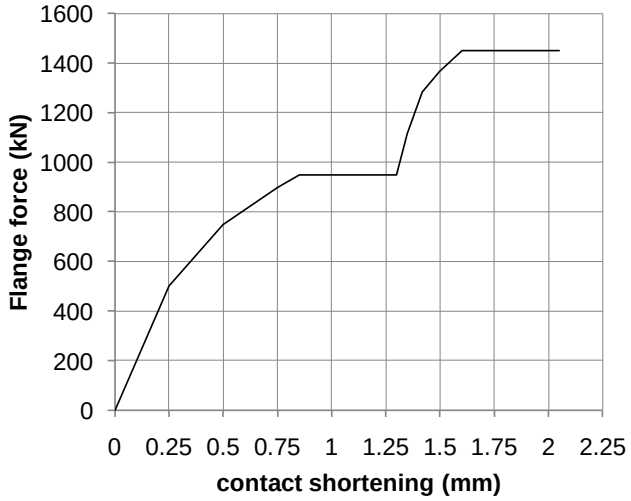

Figure 9: Skeleton curve of AG5

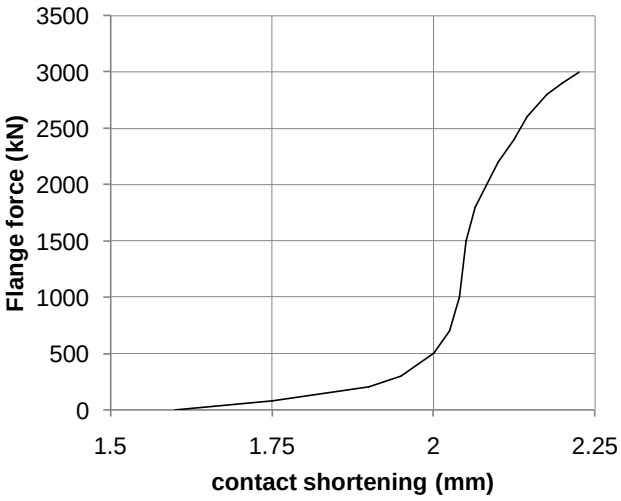

Figure 10: Monotonic curve of AG5

During the series of cyclic tests, the stresses have exceeded the elastic limit of AG5. Upon loading the specimen, the gap, filled by the AG5 material, reduces progressively. At a certain load level, the flange are in full contact with the filling. Increasing further the load provoques cruching of the AG5 material. At the end of the series of cyclic tests, a maximum displacement of 1.6 mm has been observed and crushing of the AG5 material between the two girder flange ends. After 165,700 cycles the load was increased monotonically and the behaviour of AG5 material was studied during the monotonic part of the loading of the beam-to-beam joint test specimen. The monotonic curve is given in figure 10. A total shortening of 0.65 mm was obtained at the end of the monotonic test for a maximum force of 3000 kN (which corresponds to a maximum stress of about 430 MPa and the beginning of yielding of the steel girder flanges). The measured secant initial stiffness of the contact AG5 material is about 10 000 kN/mm (with the nominal value of 70 000 MPa of the Young modulus of AG5, a stiffness of about 48 300 kN/mm would be obtained). The secant initial stiffness of 10 000 kN/mm accounts for the progressive contact during the monotonic loading between the material and the flanges.

2.5 Experimental results

Moment-rotation curves of C1 and C2 joints are given in figure 11. The final collapse occurred by failure of the shear connection of the slab close to joint C1. Stud failure was followed by the concrete cracking on the lateral face of the embedding block connecting the steel girder. The rotations considered for C1 and C2 joints are the rotations defined between the connected span section immediately adjacent to the lateral face of the concrete embedding and the cross-section of the embedding block at mid-support. They were deduced from inclinometers, beam deflections and horizontal relative displacements measured over the whole depth of the joints (Fig. 5). Moments are calculated in the connected girder cross-section from the measured actuator loads multiplied by the appropriate lever arm.

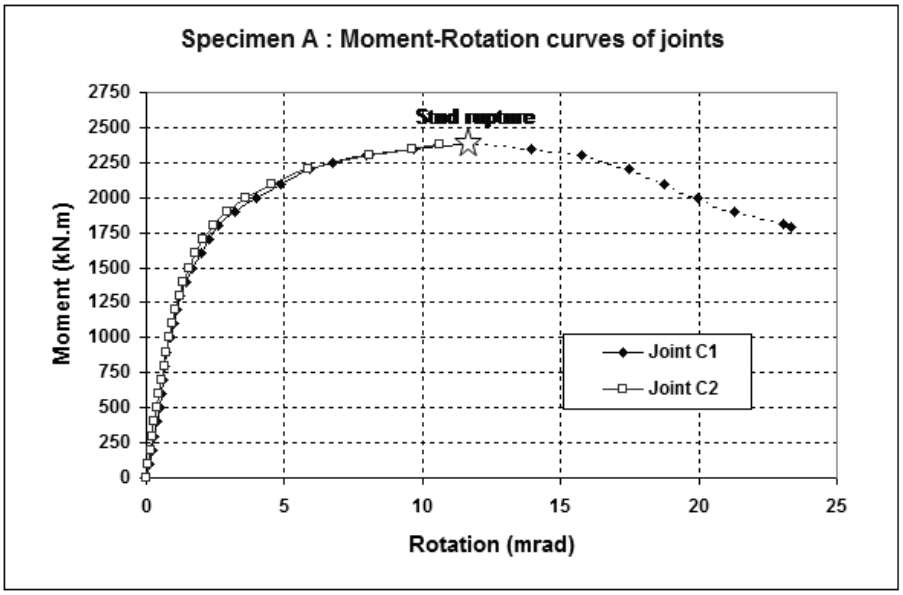

Figure 11: Moment – rotation curves of tests C1 and C2

Moment-rotation curves are very similar for both C1 and C2 joints up to the rupture of the slab shear connection on the side of joint C1. After the shear stud rupture, only joint C1 rotates. It is possible to determine from curves of figure 11 the following main characteristics for both joint C1 and joint C2: the initial mean rotational stiffness $S_{j,ini}$ *= 1125 kN.m/mrad*, the maximum exerted moment $M_{exerted}^{max}$ *= 2385 kN.m* and the moment rotation capacity which is greater than *11 mrad*. In order to better evaluate these characteristics, a comparison can be done with the corresponding characteristics of an equivalent composite beam section having the same length of about 250 mm (length of half the abutment, used to define the joint rotation). The calculated initial rotational stiffness (under flexural bending) and the elastic resistance moment of this beam segment are:

$$S_{eq} = E\, I_2 / \ell = 210\ 000 \times 140\ 558 \times 10^{4} / 250 = 1180\ kN.m / mrad \quad ; \quad M_{el,b,R} = 1842\ kN.m$$

It appears that the initial mean rotational stiffness of Joints C1 and C2 and of the equivalent composite beam segment are very close. The resistance moment of the joint is clearly higher than the resistance moment of the composite beam segment.

It is also possible to calculate the ratio $S_{j,ini}/(EI_b/L_b)$ between the joint stiffness $S_{j,ini}$ and the span stiffness (EI_b/L_b). For that, one can make the assumption that the span length L_b is equal to 1/0.15 times the span length in hogging bending of the tested specimen (Fig. 1). According to this assumption, an equivalent second moment of area $I_{eq} = 0.15 \times I_2^* + 0.85 \times I_1$ must be introduced where I_1 is the second moment of area of the effective composite cross-section under sagging

bending and I_2^* the second moment of area under hogging bending including the additional reinforcement and neglecting concrete in tension. We obtain:

$$I_{eq} = 0.15 \times 140\,538 + O.85 \times 244\,921 = 229\,264\ cm^4$$

$$\frac{S_{j,ini}}{\frac{EI_{eq}}{L_b}} = \frac{1125 \times 10^9}{\frac{210\,000 \times 229\,264 \times 10^4}{(1/0.15) \times 2\,500}} = 38{,}94$$

$$S_{j,ini} / \left(\frac{EI_{eq}}{L_b}\right) \approx 39$$

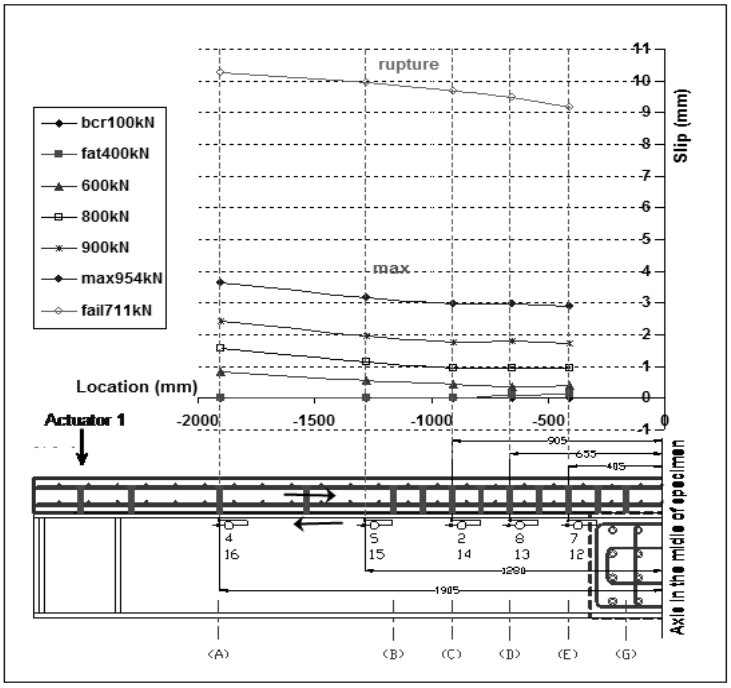

Figure 12: Joint C1: load-slip curves along the slab-steel girder interface

For joint C1, the slip distribution at the interface between the slab and the flange steel girder is given in figure 12. The slip remains quasi constant along the span girder, even a slight increase is observed when one moves from the joint section near the embedding block towards the end of the span girder. The measured average value of the slip for a load equal to 600 kN (SLS) is 0.57 mm. The deformability of the aluminium alloy piece of contact between the compressed flanges of the two steel girders is partly the cause of this slip value. In the numerical study presented in section 3, the influence of the stiffness of the contact piece on the behaviour of the connection will be analysed. To underline that the distribution of the connectors along the span is not uniform, the number of connectors between the sections (A) and (B) being half of that between the sections (B) and (G) (Fig. 12). This can explain the slight increase of the intensity of the slip, observed in figure 12, moving from the joint towards the end of the span girder.

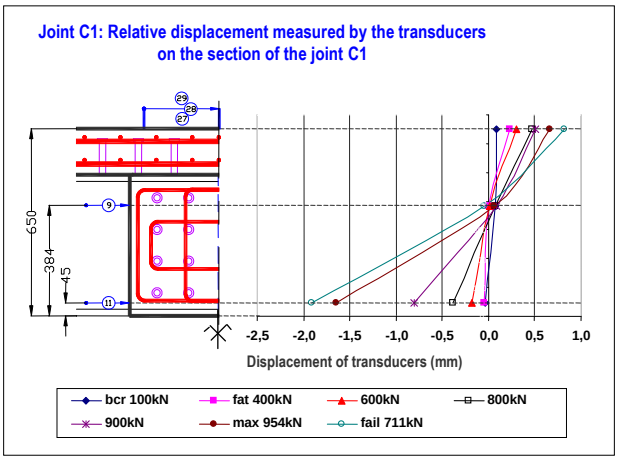

Figure 13: Relative displacement between the mid-axis of the embedding block and the girder cross-section of joint C1

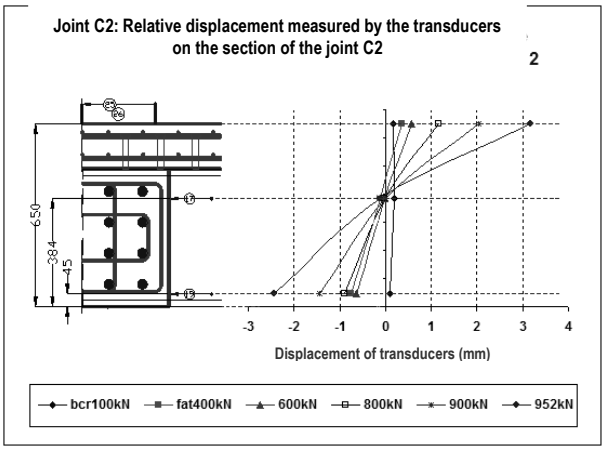

Figure 14: Relative displacement between the mid-axis of the embedding block and the girder cross-section of joint C2

Figures 13 and 14 represent the relative displacement between the mid-axis of the embedding block and the girder cross-section of joints C1 and C2, respectively. Relative displacements are more important on side of joint C2 than those on side of joint C1. The rupture occurred on side of joint C1. The rotation centre is almost at the same level for the two joined sections; maybe on the level of the higher line of shear web transversal connectors and web crossing bars.

3 NUMERICAL MODELLING

3.1 Introduction

Since the purpose of this study is to better understand the overall behaviour of such joints based on the behaviour of its main components, a 2D F.E. model involving beams and springs has been developped. The model has proved to be able to accurately reproduce the moment-rotation curve as well as the slip distribution along the beam. Furthermore, the effect of the AG5 stiffness and its degradation during cycling has been analyzed. The influence of the connection behaviour and the joint rotation has also been investigated.

3.2 Finite element software

A two-dimensional finite element model has been developed with Finelg software [13]. Finelg is a general non-linear finite element program first written by F.Frey [15] and mainly developed by V. de Ville de Goyet [16]. Specific concrete beam elements have been developed by Ph.Boeraeve [17]. The beam elements are able to simulate structures undergoing large displacements but small deformations. They are developped using a co-rotational total description.

3.3 Beam element description

A 2D Bernouilli fiber beam element with 3 nodes and 7 degrees of freedom (DOF) has been considered. The total number of DOF corresponds to: one rotational and two translational DOF for each two nodes located at beam element ends and one relative translational DOF for the node situated at mid length of the beam element (Fig. 15). The introduction of the relative translational DOF for the node at mid-length of the beam element is necessary to take into account the strong variation of the centroïd position when the behaviour of the section is not symmetric. Such situation occurs for concrete sections when cracking arises.

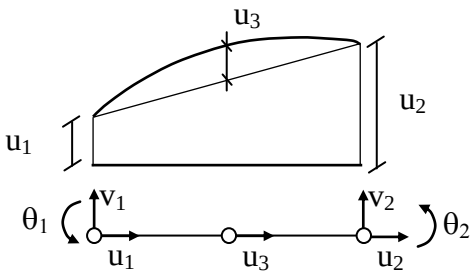

Figure 15: 3 nodes plane beam element: degrees of freedom

As usual for fibre element, the section forces at the element nodes are computed using both a longitudinal and transversal integration scheme. The integration along the beam length is performed using 4 integration points (Fig. 16a). For each longitudinal integration point (LIP_i), a transversal integration is performed using a multi-layer type scheme. The section is divided into a certain number of layers (Fig. 16b), each of which is assumed to be in uniaxial stress state. At each transversal integration point (TIP_j), the state of deformation and stress is computed.

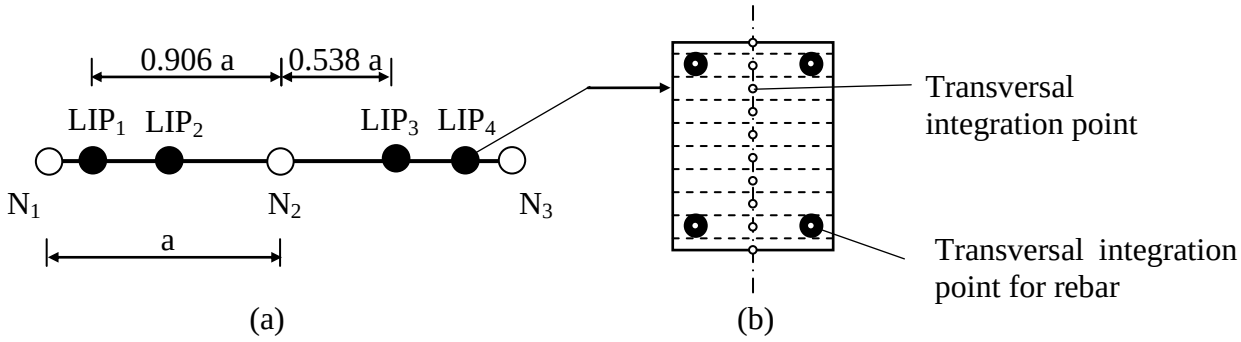

Figure 16: Integration scheme: (a) longitudinal integration with 4-point Gauss scheme; (b) transversal integration with multilayer scheme (concrete section)

The connection between the concrete beam element and the steel beam element is introduced by means of specific connection elements (Fig. 17): two transversal springs (rigidity K_y) and two rotational springs (rigidity K_Φ) to avoid uplift. Longitudinal springs are uniformly distributed along the element with ~~of~~ rigidity k_x defined from the force-slip relationship of the shear connection. The resolution of the non-linear problem is performed using classical algorithms (Newton Raphson shemes with arc length method).

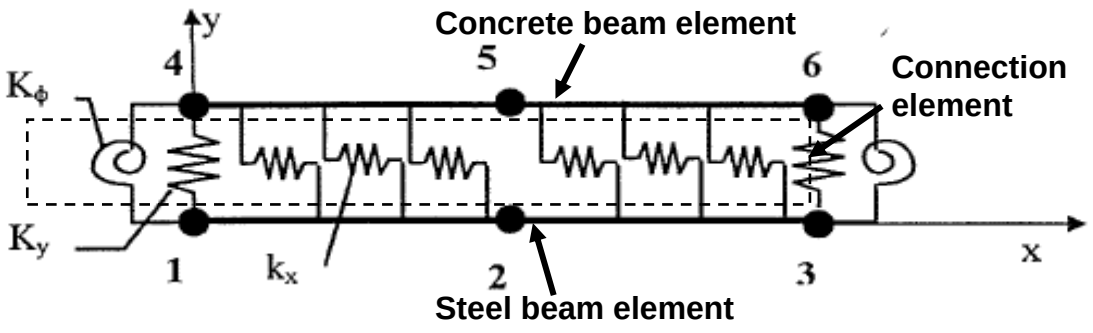

Figure 17: Plane beam and connection finite elements of FINELG

3.4 Presentation of the numerical FE model

An exploded view of the topology of the model is presented in figure 18. Three parallel lines of beam elements are considered. The two main lines: line 1 for the "concrete slab" and line 2 for the "steel girder", are continuous over the length of the specimen. Line 3 called "embedding" represents the part of concrete on the support not included in the slab. In order to give a significant mechanical meaning to this third line, an effective width of 52 cm is adopted (Fig. 18). This effective width is defined considering that the real forces in the concrete embedding block are mainly created by transmission of shear forces from the steel web to the concrete by the shear studs and the transverse reinforcement crossing through the web. This width is defined in the plane section perpendicular to the web plane by supposing that stresses propagate in the web from the bottom layers of transverse rebars (Fig. 2b) with an angle of diffusion equal to 45 °.

In each section all lines are supposed to have the same rotation and vertical displacements. A longitudinal slip is possible. Longitudinal restraints are only defined between the slab and the steel profile and between the slab and the embedding.

The length of the elements is 10 cm, except on the axis of symmetry of the specimen. The two central elements have a length of 5 mm to represent the real dimensions of the duralumin contact piece between the bottom flanges.

Nominal geometrical characteristics and real measured mechanical characteristics are adopted for the finite element modeling of the HEA 500 steel profile: Young modulus E_s = 200 000 MPa and mean yield strength f_y = 430 MPa. Isotropic hardening modulus is set to $E_h = E_s/100$ = 2 000 MPa (Fig. 18).

The tensile strength of the first steel elements next to the duralumin element is set equal to 0 MPa. Only compressed fibers are stressed in order to model the interruption of the steel profile and to better take into account the real diffusion of stresses from the contact area to the whole section.

The material behaviour of the duralumin is supposed to follow a Ramberg-Osgood law (R-O law) :

$$\varepsilon = \frac{\sigma}{70000} + 0.002 * \left(\frac{\sigma}{150}\right)^{3.5} \quad \text{with } \sigma \text{ in MPa.} \qquad (1)$$

The mean compressive strength of the concrete, obtained from cylinder tests, is 56 N/mm2. For concrete under compression, a parabolic stress-strain relationship is used (Fig. 18).

All parameters except the resistance are deduced from Eurocode 2. In tension an elastic linear law is assumed up to half-experimental tensile strength, then a linear softening branch models the tension stiffening effect. At $\varepsilon = 0.00215$, the stress is taken equal to 0.

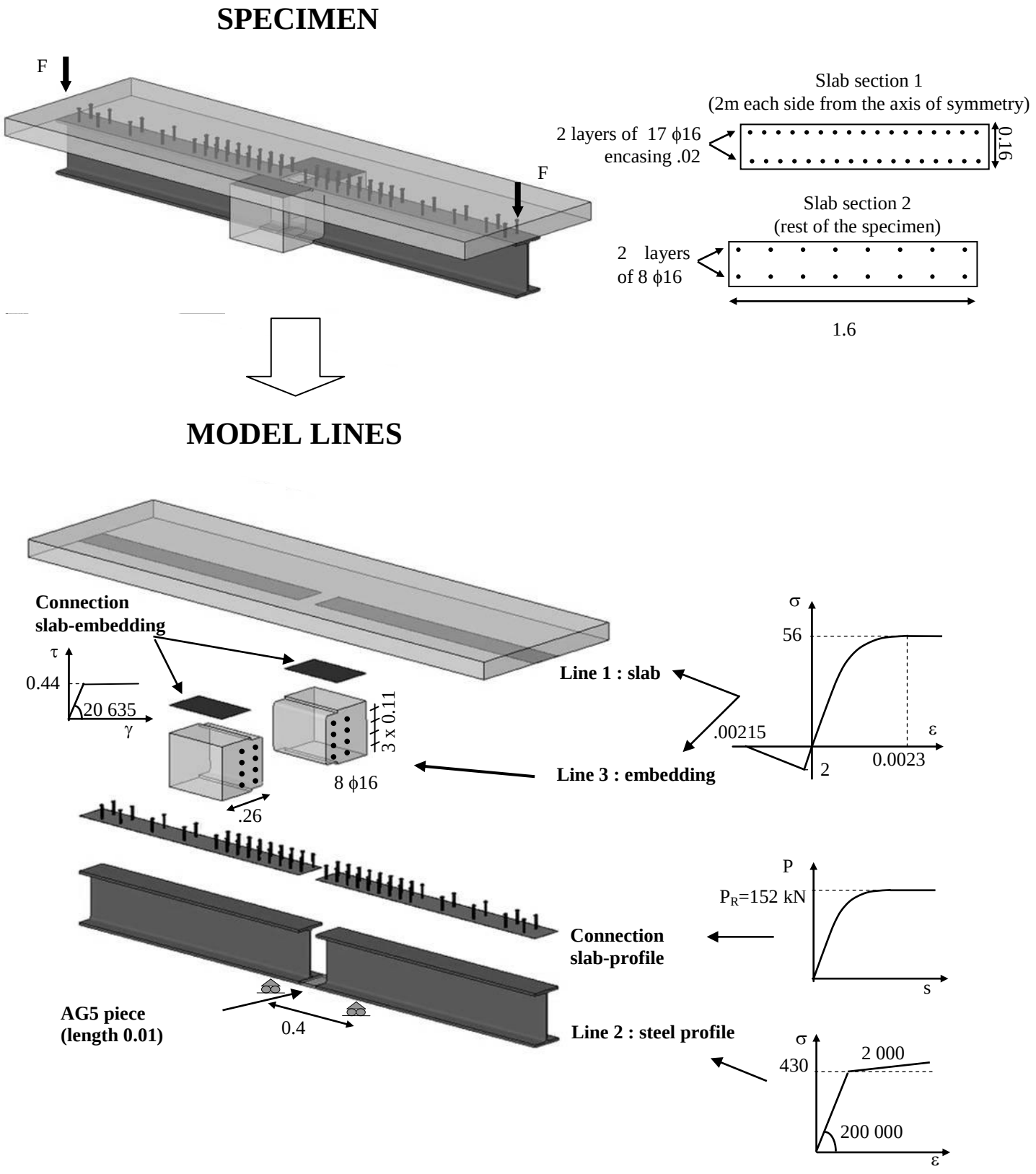

Figure 18: Lines of longitudinal elements and sliding connections (Units : MPa and m)

The measured tensile strength of rebars is 580 MPa. Young and hardening moduli are taken equal to the values adopted for the steel profile, respectively.

The stud resistance P_R = 152 kN has been adopted. Force-slip relationship (P-s) of studs has been chosen according to a recent experimentation conducted at Wuppertal University [19] :

$$\frac{P}{P_R} = \left(1 - exp\ \left(-1.22\ s^{0.59}\right)\right);\ \text{with } s \text{ in mm} \qquad (2)$$

The location of the studs connecting the profile to the slab is shown in figures 2a, b, c and 18.

In order to model suitably the shear behaviour at the interface between the slab and the embedding a fictitious horizontal plane connecting the two parts is introduced. Its shear resistance is taken equal to 0.44 N/mm². An elastoplastic behaviour is considered with a shear modulus G = 20 600 MPa.

The load is applied at both specimen ends. Supports are defined under the lower flange by extra nodes connected to the steel beam elements by rigid links.

3.5 Numerical results

In figure 19, the experimental moment-rotation curves of C1 and C2 joints (Fig. 11) are compared against two numerical simulations. In the first simulation, the Ramberg-Osgood law defined by Eq. (1) is used with a nominal Young modulus E_0 = 70 000 Mpa (let us recall that the corresponding elastic initial stiffness of the contact AG5 material is 48 300 kN/mm). The so-obtained numerical curve gives a larger initial stiffness and larger resistance than the experimental curve. In the second simulation the cyclic damage of the AG5 contact material is taken into account. As seen in the previous paragraph 2.4 and shown in figure 7, during the initial cyclic fatigue loading, cumulative plastic damage deformations developed cycle after cycle (ratcheting) in addition to the gap reduction of the AG5 material between the two girder flange ends and led to a total shortening of 1.6 mm of the contact piece thickness. So, introducing in the second simulation an equivalent stiffness modulus, calibrated from experimental results (Fig. 9 and 10) to the value of 759 kN/mm (which corresponds to an equivalent elastic modulus of 1 100 Mpa), in order to take into account the initial cyclic shortening in addition to the monotonic elasto-plastic deformation of the contact material, the new curve (Fig. 19) follows more closely the experimental one. This equivalent secant stiffness value, associated to a linear law, was kept for the rest of the study.

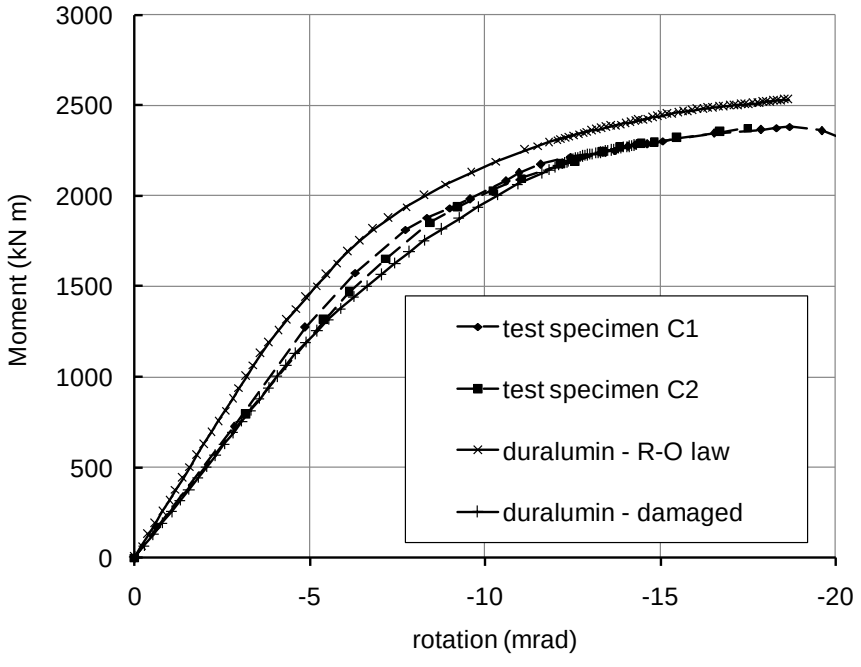

Figure 19: Effect of cyclic damage of contact

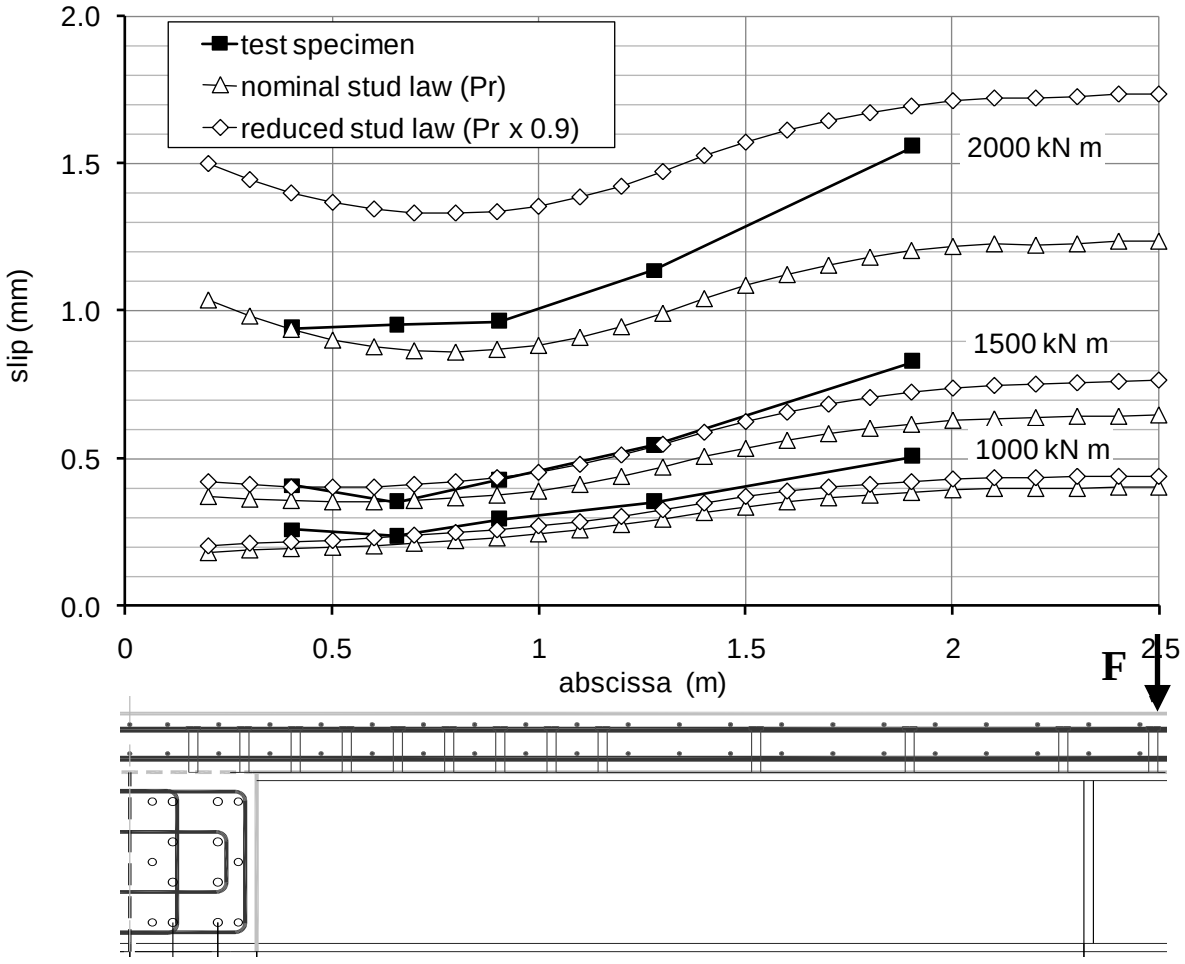

Figure 20: Slip with variable numerical stud characteristics

In figure 20, experimental slips measured along the slab-to-beam interface are compared to two simulations: one with the nominal resistance of the studs (P_R = 152 kN), and the other one with 0.9 P_R (cf. Eq. (2)). Large differences appear between the two numerical simulations. For a load level near collapse (M = 2000 kN.m), the mean slip is around 1 mm when the nominal resistance of the studs is adopted, while it grows up to 1.5 mm when the resistance of the stud P_R is decreased from 10 %. This influence of the stud law's uncertainty on slip results must be underlined. It is the consequence of the high work rate of the studs near collapse. Nevertheless the global behaviour of the joint seems to be not affected by the variation of the stud resistance characteristic (Fig. 21).

In order to better evaluate the influence of the joint on the continuity of a bridge composite beam, three numerical moment-rotation curves are presented in figure 22:

- a first one for a continuous composite beam without joint over the support ;
- a second one with the joint (nominal stud law P_R) ;
- the third one is the same as the previous one without concrete embedding.

It appears that at serviceability limit state (P = 450 kN), the discontinuity due to the joint induces a flexibility characterised by an increase of the vertical displacement of 35 %. The effect of the joint stiffness is thus not negligible and it has to be taken into account in the bridge design. From

another point of view, the stiffness of the joint induces a favorable effect in making easier the redistribution of bending moments from the support to midspan regions.

The effect of the concrete embedding has been evaluated in figure 22. Without embedding, the initial rotational stiffness is reduced by about 20% compared to the joint with embedding and 60% compared to the continuous beam. Without embedding, the maximum moment is reduced by 15% compared to the joint with embedding and 25% compared to the continuous beam.

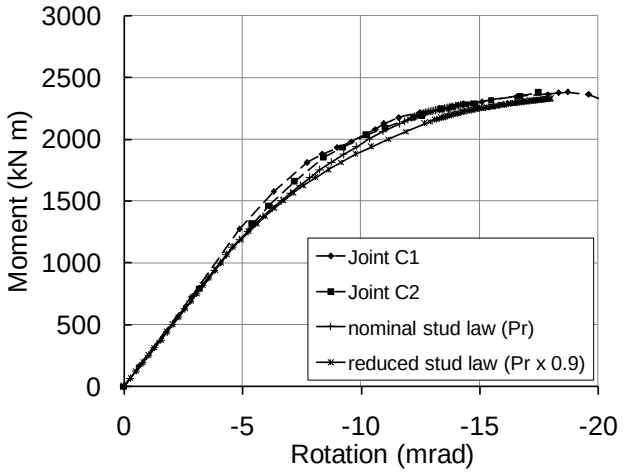

Figure 21: Effect of stud resistance characteristics

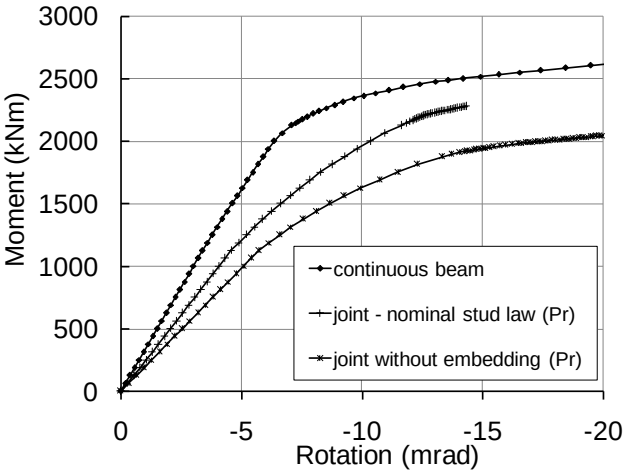

Figure 22: Additional rotation due to the joint

4 EFFECTS OF THE PRESENCE OF A BEAM-TO-BEAM EMBEDDED JOINT ON THE GLOBAL BEHAVIOUR OF A DECK IN A COMPOSITE BRIDGE

4.1 Introduction

A two span composite bridge is chosen as worked example to examine the effect of the presence of a beam-to-beam joint on the global behaviour of the deck. For that, a comparison is made between a continuous deck and the same deck with a beam-to-beam embedded joint located on the intermediate pile. The stiffness and the resistance of the joint may introduce a local behaviour able to modify the distribution of bending moments in the deck and therefore it should be taken into account in structural analysis if necessary. In the following paragraphs 4.2, 4.3 and 4.4 the study is carried out in two stages. A first stage involves the predesign of the bridge using for that a commercial software, easier to use but which does not allow to introduce in the calculation the studied joint presented in this paper. So, in a second stage a specific FE model based on Finelg software is developped to study the effects of the behaviour of an embedded joint on the distribution of internal forces and moments within the deck of a composite bridge.

4.2 Predesign of the two-span bridge taken as worked example

The worked example chosen is a two-span continuous railway bridge with two railroad tracks (Fig. 23). Each span is considered 20 m long.

Calculation of overall dimensions is made through Acobri software [14]. This software can be used for manual or automatic predesign of the main beams of the superstructure of a composite steel and concrete bridge. The bridge types covered are the following: road bridges, railway bridges, footbridges. Structural analysis is performed using a grillage-type model, then SLS and ULS verifications are made in accordance with the ENV or the French code.

For this example the predesign is made following the ENV, considering the grade S355 for steel and the class C35/45 for concrete. The design resulting from Acobri Software leads to a transversal section made of 4 steel profiles HL 1100 R supporting a deck 0.3 m thick (Fig. 24). The rebar

density is 1 % along the whole length of the bridge. 2/3 of the rebars are put in the top layer and 1/3 in the bottom one. The concrete cover is 0.04 m measured at the axis of the bars.

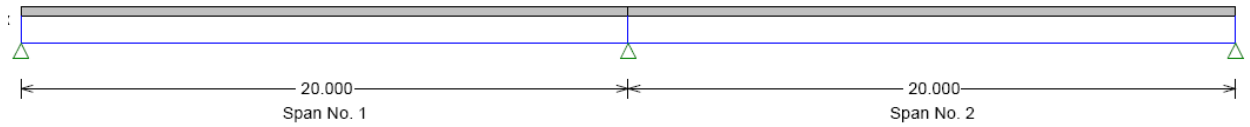

Figure 23: Elevation of the bridge

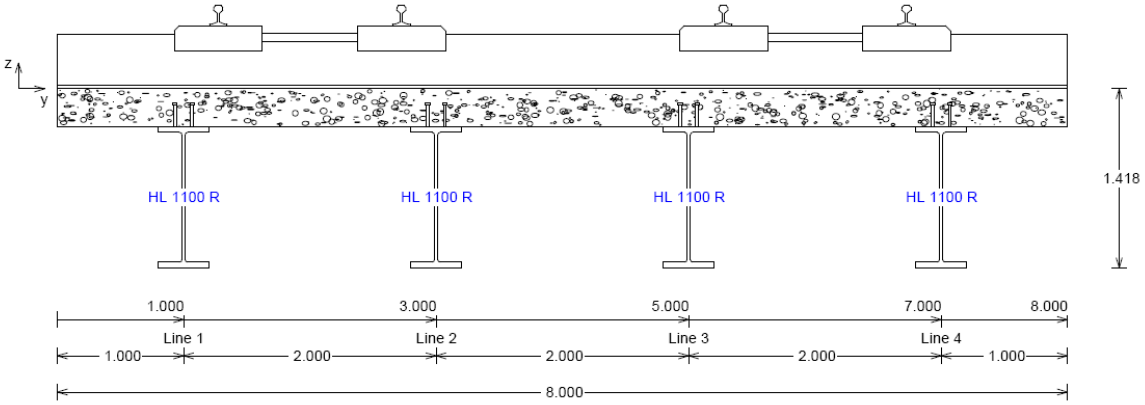

Figure 24: Cross-section of the deck

The resulting total permanent load is about 6000 kN. The corresponding load on each steel profile is 37.5 kN/m. The maximum hogging bending moment at ULS is M_{Ed} = 7750 kNm. The bending work rate at ULS is higher on the pile than in the span :

$$M_{Ed,pile} / M_{Rd,hogging} = 0.82$$

$$M_{Ed,span} / M_{Rd,sagging} = 0.53$$

with $M_{Ed,\ pile}$ and $M_{Ed,span}$ being the maximum ULS moments in hogging and in sagging, and $M_{Rd,hogging}$ and $M_{Rd,\ sagging}$ the corresponding resisting moments.

At SLS, the maximum work rate is obtained for the verification of the maximum stress in rebars :

$$\sigma_{s,rebar,pile} / 0.8\ f_{sk} = 0.96$$

With f_{sk} being the nominal resistance of the reinforcement bars, and $\sigma_{s,rebar,pile}$ the maximum stress in the rebars over the piles.

For displacement and rotation criteria, the work rate is below 0.7.

4.3 Characteristics of the embedded joint

Usually, in a the global analysis, a joint is represented by a rotational spring connecting the centre lines of the connected members. In the case of a beam-to-beam joint configuration, as indicated in figure 25, two joints and so two rotational springs are considered on each side of the mid-axis of the support. Each end-side joint characteristics are gathered in the rotational spring and expressed in the

form of a moment-rotation curve that describes the relationship between the bending moment $M_{j,Ed}$ and the corresponding rotation Φ_{Ed}. Such a curve was obtained in paragraph 2 from the experimental tested specimen. A relative rotational stiffness $S_{j,ini}/(EI_{eq}/L_b) = 39$ was obtained from the test.

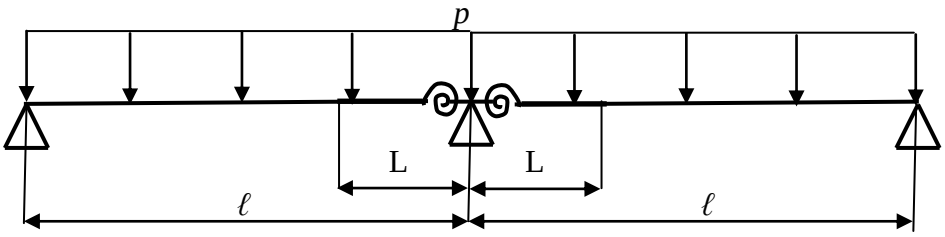

Figure 25: Bridge structural scheme with embedded joint

The design of an embedded joint as the one presented in this paper requires the implementation of additional rebars in the slab and additional studs at the slab-girder flange interface. It was the case of the experimental specimen presented in paragraph 2 where additional rebars and studs were installed over a length equal to 1.8 meters on each side from the mid-axis of the support. In order to develop the most accurate model, this local strengthening over a corresponding length L = 0.2 l adjacent to the rotational springs will be taken into account in the worked example model (Fig. 25).
The supplementary longitudinal reinforcing bars of the slab have deen designed from the maximum ULS hogging bending moment :

$$A_s = M_{Ed} / (f_{yd} (h_{profile} + ½ h_{deck}))$$

$$A_s = 7750 /(1.27\ 435000) = 14000\ mm^2$$

4.4 Effect of the joint characteristics on the bridge behaviour

In order to study the effects of the joint characteristics on the bridge behaviour, a FE model is developped using Finelg software. It is made with plane beam elements, considering 10 steel elements and 10 concrete elements in each span. The steel-deck connection is supposed to be rigid. As said previously and shown in figure 25, two springs are introduced on each side of the mid-axis of the support to model the embedded joint. ***

Non-linear computations are carried on to take into account the redistribution due to cracking.

In order to study the effects of the joint characteristics on the global bridge behaviour, the joint stiffness is introduced in the model as a variable parameter.
To cover both ULS and SLS, two load cases are considered:

- Uniform loading of both spans to obtain the maximum negative moment at ULS on the support. Load is computed to obtain the same negative moment than in predesign. However it will never be reached in this computation because of the redistribution due to cracking;
- Uniform loading of one span with a load of 40 kN/m to verify the SLS deflections under variable loads. This is half of the UIC and it is representative of the part of the load applied on one profile for this four girder – double railway track bridge at SLS.

Figure 26 gives the variation of the maximum deflection versus joint stiffness values. The maximum deflection corresponding to the hypothesis of a continuous beam is represented in the figure by a line parallel to x axis. At SLS, it appears that the effect of the joint on the maximum deflection of the span is negligible (Fig. 26): for a relative rotational stiffness of the joint $S_{j,ini}/(EI_b/L_b) = 39$, the deflection increases by about 0.25 mm (3 %).

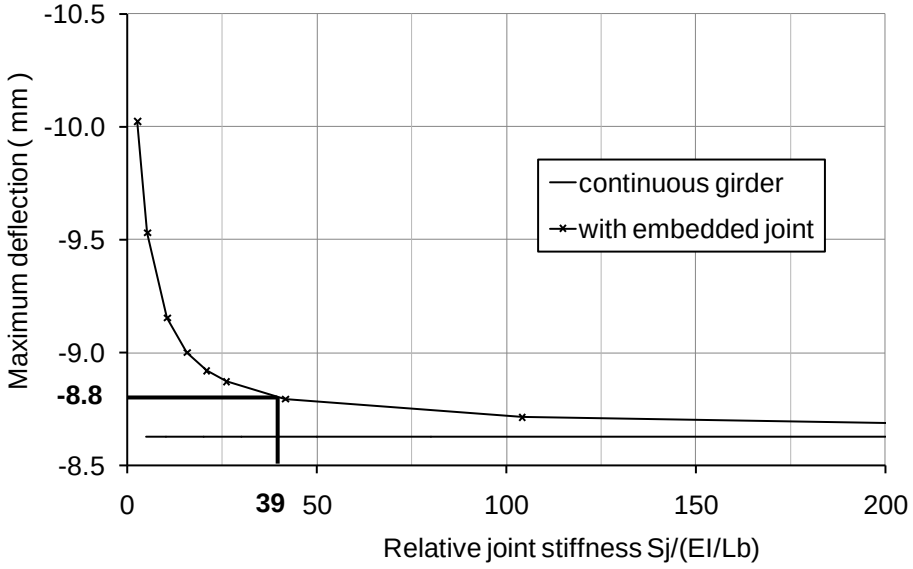

Figure 26: Effect of the relative joint stiffness on maximum SLS deflection

The variation of the hogging bending moment on the support at ULS is a little bit more important (Fig. 27). Bending moment is reduced by about 10 % for the relative joint stiffness $S_{j,ini}/(EI_b/L_b) = 39$.

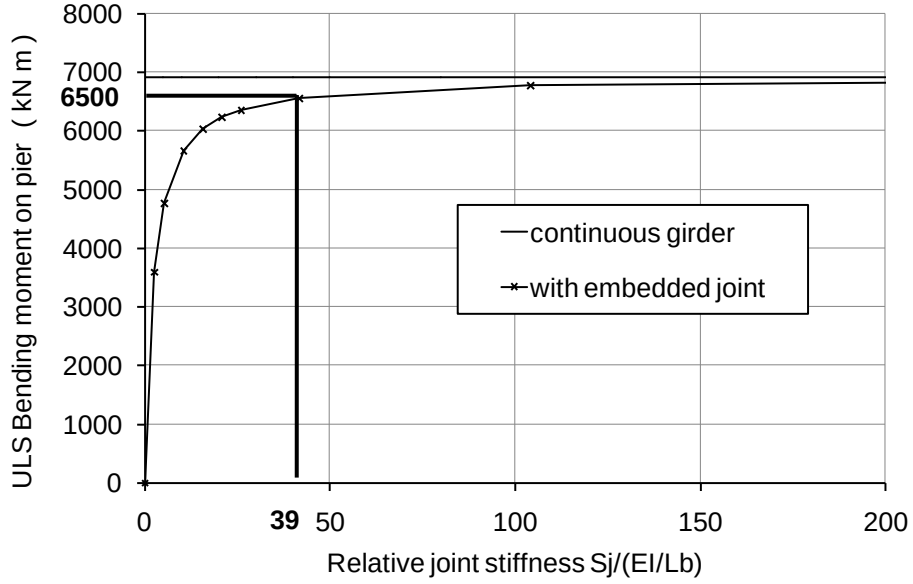

Figure 27: Effect of the relative joint stiffness on bending moment on support

For the small span bridge taken as example in this paragraph, figures 26 and 27 show that a variation of the relative joint stiffness between 25 and 200 gives a variation of the maximum deflection and of the maximum hogging bending moment less than 10%. This result seems to show that the global behaviour of the bridge is not so affected by the beam-to-beam joint stiffness. However, it seems desirable to reach through the joint design a relative rotational stiffness value lower than the one of the continuous composite beam in order to not amplify the hogging bending moment at the support and to allow the redistribution effect of bending moments in the composite beam. To point out that for such small span bridge the hogging bending moment zone on the support is the more often decisive for the design of the continuous composite beam.

5 CONCLUSION

In this paper a new type of beam-to-beam composite joint has been presented. This joint was realized by encasing totally the two ends of adjacent span composite beam into the massive transverse concrete reinforced block resting on the bridge piles. New devices were developed to connect with shear anchors or transverse rebars the end steel girders in the concrete and to ensure by direct contact the transfer of compressive forces between the bottom steel flanges of the girders. An experimental study showed first that such a type of joint was able to connect continuously composite beams in small and medium span bridges and to develop a regular increasing monotonic moment-rotation behaviour. The fatigue resistance of such a joint was also investigated. The measured initial rotational stiffness and the resistance moment have indicated that such a joint was rather rigid and full strength. Other experimental results as relative displacements inside the joint or slip along the interface between the concrete slab and the steel flange girder showed a regular transfer of the internal forces inside the joint.

In addition to the experimental study, a finite element model has been developed. Despite the spatial nature of the joint, it was found that a 2D numerical beam model is able to reproduce the global behaviour of the beam-to-beam composite joint and to give valuable insight. The influence of some parameters on the global behaviour of the joint has been studied. Thus, the sensitivity of the stiffness of the AG5 contact material has been evaluated. A secant stiffness of the contact material to be introduced in a numerical model has been proposed. The influence of some parameters introduced in the force-slip law of the studs was also examinated. It has been shown a great sensitivity of the value of the resistance P_R on the slip amplitude along the slab-to-flange girder interface and, conversely a small effect of the value of the resistance P_R on the global moment-rotation behaviour of the joint. The effect of the presence of concrete in the joint could be examined from the numerical model. It has been obtained that in a same joint without concrete the initial rotational joint stiffness was divided by two and the maximum moment resistance reduced by 15%.

The third part of this paper was devoted to the study of the effect of the embedded beam-to-beam joint investigated in this research on the global behaviour of the deck of a composite bridge. The selected worked example was a two-span composite railway bridge with a 4 multi-beam cross section of the deck. At SLS, it appeared that the embedded joint characteristics determined previously from experimental measurements led to negligible variations of the maximum deflection at mid-span compared to the maximum deflection obtained in the case of a continuous deck without joint. In addition, numerical results dealing with the influence of the rotational stiffness on the global behaviour of the bridge seems to show that for a large range of relative rotational stiffness values, the overall behaviour of the bridge is unaffected. However it seems desirable to have for the joint an initial rotational stiffness which stays near the rotational stiffness of the connected composite beams to avoid hogging bending moment amplification at support and to allow the redistribution of bending moments between hogging and sagging zones of the composite beam.

ACKNOWLEDGEMENTS

The authors would like to thank IREX, the "French Ministry of Ecology and Sustainable Development", ArcelorMittal-Research and SNCF-Engineering for their financial and technical support through the national project MIKTI.

REFERENCES

[1] Fried A., *New type of composite steel and concrete bridge,* Acier-Stahl-Steel, 11/1974.

[2] Van der Meer A.T. and Palmer P.M., *Concrete connection for steel bridge beams*, ARRB proceeding, volume 9, part 4, Western Australia, 1978.

[3] Kell R.A., Fried A. and Lloyd J.K., *Steel bridges using concrete infill sections to achieve continuity, Int. Conf. On short and medium span bridges*, Toronto, pp 159-169, 1982.

[4] Smith A.J., Current and future steel bridge construction in NSW, Journal of the Australian Institute of Steel Construction, Vol. 15, N°4, 1981.
[5] Lloyd J.K. and Kell R.A., Steelwork – An appropriate material for small to medium span bridges in developing countries, International conference on materials for developing countries, University of New South Wales, 1981.
[6] Ivering J.W., *Connecting short-span steel girders for continuity*, IABSE Symposium Leningrad, 1991.
[7] Wang J., Baus R., Bruls A., Bolted Connections of Hot Rolled Beams in Composite Bridges, *Conference report Innsbruck Composite Construction,* 1997.
[8] Haensel J., Recent trends in composite bridge design and construction in germany, 554-565, avril 2001.
[9] RWTH-CTICM-PROFILARBED, Composite Bridge Design for Small and Medium Spans, *ECCS STEEL RTD PROGRAMME (CECA) Interim Report N°2*, 2000.
[10] Lachal A., Aribert J.M., National program MIKTI, Conception de tabliers performants dans le domaine des petites portées, Sujet 1-B : Techniques innovantes de raboutage, Cahier des charges. *Research report,* février 2002.
[11] Lachal A., Kaing S.S., Guezouli S., Somja H. and Aribert J.M., National program MIKTI, Innovative beam-to-beam solutions, chapter 1.2 of the book : Steel-concrete bridges, a guide for novel structures, edited by B. Chabrolin, Th. Kretz and J. Laravoire, Presses des Ponts, Paris, 2010.
[12] ASCE Task Committee on Design Criteria for Composite Structures in Steel and Concrete. Guidelines for design of joints between steel beams and reinforced concrete columns. Journal of Structural Engineering, Vol.120, No. 8, August, 1994, ASCE
[13] FineLg User's Manual, V9.2. Greisch Info – Department ArGEnCo – ULg (2011).
[14] Acobri ACOBRI, ArcelorMittal Composite Bridges, Version 2.05. To be downloaded at www.arcelormittal.com/sections/ . 2008
[15] Frey F. "L'analyse statique non linéaire des structures par la méthode des éléments finis et son application à la construction métallique". *Doctoral thesis*, Université de Liège, 1977.
[16] de Ville V., L'analyse statique non linéaire par la méthode des éléments finis des structures spatiales formées de poutres à section non symétrique. *Doctoral thesis*, Université de Liège, 1989.
[17] Boeraeve P.: Contribution à l'analyse statique non linéaire des structures mixtes planes formées de poutres, avec prise en compte des effets différés et des phases de construction. Doctoral thesis, Université de Liège, 1991.
[19] Hanswille G., Pörsch M, Ustundag C., Resistance of headed studs subjected to fatigue loading, *Journal of Constructional Steel Research 63, 485-493*, 2007.